Non-Stationary Dynamics of Compound Climate Extremes: A WRF-CMIP6-GAMLSS Framework for Southeastern China

Yinchi Zhang[1, 2, 3, 4], Wanling Xu[5], Chao Deng[6], Shao Sun[7], Miaomiao Ma[8], Jianhui Wei[10], Ying Chen[1, 2, 3, 9], Yi Wang[4], Lu Gao[1, 2, 3, 9*], Harald Kunstmann[10, 11, 12]

[1]*Key Laboratory for Humid Subtropical Eco-geographical Processes of the Ministry of Education, Fujian Normal University, Fuzhou, 350117, China*

[2]*Institute of Geography, Fujian Normal University, Fuzhou, 350117, China*

[3]*School of Geographical Science, Fujian Normal University, Fuzhou, 350117, China*

[4]*Department of Geography and School of Global Studies, University of Sussex, Falmer, Brighton BN1 9RH, UK*

[5]*School of Ocean and Earth Science, Tongji University, Shanghai, 200092, China*

[6]*Sichuan Academy of Forestry Sciences, Chengdu, 610081, China*

[7]*State Key Laboratory of Severe Weather, Chinese Academy of Meteorological Sciences, Beijing 100081, China*

[8]*China Institute of Water Resources and Hydropower Research, Beijing, 100038, China*

[9]*Fujian Provincial Engineering Research Center for Monitoring and Accessing Terrestrial Disasters, Fujian Normal University, Fuzhou, 350117, China*

[10]*Institute of Meteorology and Climate Research (IMKIFU), Karlsruhe Institute of Technology, Campus Alpin, Garmisch-Partenkirchen, Germany*

[11]*Institute of Geography, University of Augsburg, Augsburg, 86159, Germany*

[12]*Centre for Climate Resilience, University of Augsburg, Augsburg, 86159, Germany*

***Corresponding Author: Lu Gao, l.gao@foxmail.com**

Abstract

Understanding future changes in compound climate extremes (CCEs) is critical for climate risk assessment. Existing research, however, has largely relied on stationary assumptions, overlooking the dynamic evolution of CCEs under non-stationary climate change. To address this gap, this study employs an enhanced Generalized Additive Model for Location, Scale, and Shape (GAMLSS) framework to provide novel insights into the non-stationary characteristics of hot-wet (HW), hot-dry (HD), cold-wet (CW), and cold-dry (CD) extremes under future climate scenarios. We focus on the Minjiang River Basin (MRB) in Southeast China. A high-resolution dataset for CEE detection was generated by dynamical downscaling a bias-corrected CMIP6 dataset, using the Weather Research and Forecasting (WRF) model. Our results indicate that (1) CCEs increase significantly at a rate of 3.55 days per decade under the SSP5-8.5 scenario, with hot extremes (HW and HD) being the dominant contributors. Spatially, the increases exhibit a distinct west to east gradient, peaking in the downstream areas of the MRB. (2) Under the SSP5-8.5 scenario, CCEs exhibit a marked shift from stationary to non-stationary characteristics, with non-stationarity detected in 95.20% of grid cells. This transition is primarily driven by mean warming, which explains 80.81% of the change, rather than by variability. (3) The non-stationary results demonstrate that the severity and recurrence frequency of CCEs are systematically underestimated under stationary assumptions. Most CCE types (except for CD) show an increasing recurrence frequency under the SSP5-8.5 scenario. For instance, the frequency of events with a 100-year return period increases at a stronger trend of 3.12 days per decade. This study emphasizes the necessity of updating the frequency changes of CCEs under a non-stationary framework.

Keywords compound climate extremes, non-stationarity, GAMLSS, dynamical downscaling, WRF

1 Introduction

Global warming is leading to more frequent and intense compound climate extremes (CCEs) (Sauter et al., 2023; Liu et al., 2024; Zhang et al., 2024; You et al., 2025). CCEs have posed severe threats to global social, economic, and ecological systems, with impacts that surpass those of individual extremes in both range and severity (Mukherjee et al., 2023; Zeng et al., 2024; Miao et al., 2024). For example, the Yangtze River Basin in China experienced unprecedented compound hot-dry extremes in August 2022, characterized by record-breaking heatwaves and severe droughts, which directly affected over 50 million people (Jia et al., 2025). The Sixth Intergovernmental Panel on Climate Change (IPCC) report indicated that the probability and intensity of future CCEs are projected to increase (IPCC, 2021). Therefore, a systematic assessment of the future evolution of CCEs is critical for mitigating socio-economic risks and optimizing climate adaptation strategies.

Recent studies have increasingly focused on CCEs, highlighting their growing significance in the context of climate change. Zscheischler et al. (2018) were the first to clearly define the concept of compound events, emphasizing how the interaction of multiple climate and meteorological drivers can amplify extreme impacts. Building on this, Ridder et al. (2022) conducted the first global-scale assessment of the changes in compound events, specifically examining the co-occurrence of heatwaves and drought, extreme winds, and precipitation. Wu et al. (2023) revealed that under warming conditions, the risks associated with global compound pluvial–hot extreme events are projected to be significantly greater in the future than those observed during the historical period. Fang et al. (2025) investigated the future changes of sequential heatwaves and precipitation events as well as concurrent drought and heatwave events in China, with projections indicating an increase in both the frequency and intensity of these events.

While large-scale studies play a crucial role in advancing our understanding of global climate change and extreme events, their practical relevance for disaster risk management and adaptation strategies in medium- and small-scale regions is relatively limited due to their lower spatial and temporal resolution. To overcome this constraint, dynamical downscaling, which utilizes nested high-resolution regional climate models (RCMs), provides a critical technical pathway to investigate climate response mechanisms at fine-scales (Tapiador et al., 2020; Rahimi et al., 2024). Compared to Global Climate Models (GCMs), RCMs offer higher spatial resolution, allowing for

more precise simulations of local climate effects induced by topography, such as local convective precipitation, orographic effects, and regional climate heterogeneity (Gilbert et al., 2025). In regions with complex terrain, RCMs are particularly effective at capturing spatial variations of climate variables, such as the differences in wind patterns, precipitation, and their distribution caused by topography in mountainous or basin areas (Imran and Evans, 2025). For example, Byun et al. (2023) assessed the ability of RCMs and GCMs to simulate storm tracks in East Asia, revealing that RCMs are better able to capture high-resolution topography, thereby reducing the biases found in GCMs. Lin et al. (2022) showed that RCMs driven by ERA-Interim reanalysis data are capable of capturing small-scale processes, such as orographic effects, and outperform GCMs in reproducing the large-scale features of the Heat Wave Magnitude Index-daily. Torrez-Rodriguez et al. (2023) also demonstrated that RCMs are better at reproducing the main spatio-temporal characteristics of precipitation in subtropical complex terrain regions. As an advanced convection-permitting RCM, the WRF model significantly enhances the simulation capability for meteorological processes at 1-10 km scales through its fully compressible, non-hydrostatic dynamic core framework (Talbot et al., 2012). This high-resolution simulation capability gives the WRF model a unique advantage in capturing small-scale meteorological phenomena. Zhou et al. (2024) developed a 9 km resolution regional reanalysis dataset covering the Tibetan Plateau based on the WRF model, and demonstrated its superior applicability compared to the fifth generation European Centre for Medium-Range Weather Forecasts Reanalysis (ERA5). Yang et al. (2024) revealed that the WRF model provides better accuracy in simulating snow depth during the cold season in high-elevation regions compared to ERA5-Land.

Additionally, traditional extreme event analyses rely on stationarity assumptions (when analyzing time series data, it is assumed that the statistical properties of the series remain constant over time), presuming that the probability and distributional parameters of climate variables are constant (Sun et al., 2018; Nerantzaki et al., 2023). However, driven by synergistic effects of global warming and anthropogenic forcing, extremes exhibit significant shifts in distributional characteristics (Gao et al., 2018). Therefore, traditional models fail to capture the non-stationary (the statistical properties of a time series change over time and do not remain constant) changes in these extreme events. Many studies have applied the Generalized Additive Models for Location,

Scale, and Shape (GAMLSS) (Rigby and Stasinopoulos 2005) to address non-stationary problems in hydrological and meteorological extremes, enabling updated risk analysis of evolving climate extremes. Lei et al. (2021) investigated the non-stationary changes of extreme precipitation in the Poyang Lake Basin and found that the stationary assumption underestimates the intensity of extreme precipitation in this region. Shao et al. (2022) innovatively proposed the Nonstationary Standardized Runoff Index (NSRI), and the results indicate that, compared to the stationary index, it can more accurately identify drought events. Salarijazi et al. (2023) evaluated the nonstationarity of maximum temperatures in multiple urban areas of Iran and concluded that traditional stationary approaches tend to underestimate the risk of annual maximum temperatures. However, existing non-stationary analyses only focus on individual extremes, and the potential non-stationarity of CCEs has not been established. The comprehensive assessment of future changes in CCEs within a non-stationary framework is also lacking.

To address these research gaps, this study adopts a high-resolution approach by integrating the WRF model with GAMLSS. We first perform dynamical downscaling using the WRF model to refine the bias-corrected Coupled Model Intercomparison Project Phase 6 (CMIP6bc) data (1.25° × 1.25°) to a 3 km resolution. Based on these high-resolution WRF outputs, CCEs are then identified and used as input for the GAMLSS framework to analyze their non-stationary characteristics. This methodology overcomes the limitations of traditional coarse-resolution models and addresses the shortcomings of stationary assumptions in CCE analysis. By focusing on the Minjiang River Basin (MRB)—a subtropical, monsoon-dominated basin in southeastern China where complex topographic–climatic interactions give rise to high-intensity compound hydroclimatic extremes (Gan et al., 2025; Geng et al., 2024; Wang et al., 2024)—this research aims to examine four types of CCEs: hot-wet (HW), hot-dry (HD), cold-wet (CW), and cold-dry (CD) events. The analysis proceeds as follows (Figure 1): Supplement Section S1 presents the validation of CMIP6bc applicability. Section 3.1 characterizes the spatio-temporal patterns of CCEs under both a middle-of-the-road scenario (SSP2-4.5) and a high-emissions scenario (SSP5-8.5). The non-stationarity detection of CCEs is described in Section 3.2. The recurrence frequency changes in CCEs under non-stationary conditions is evaluated in Section 3.3. The work establishes a scientific basis for addressing the environmental and climatic challenges posed by CCEs, thereby

contributing to effective strategies for regional sustainability and climate resilience.

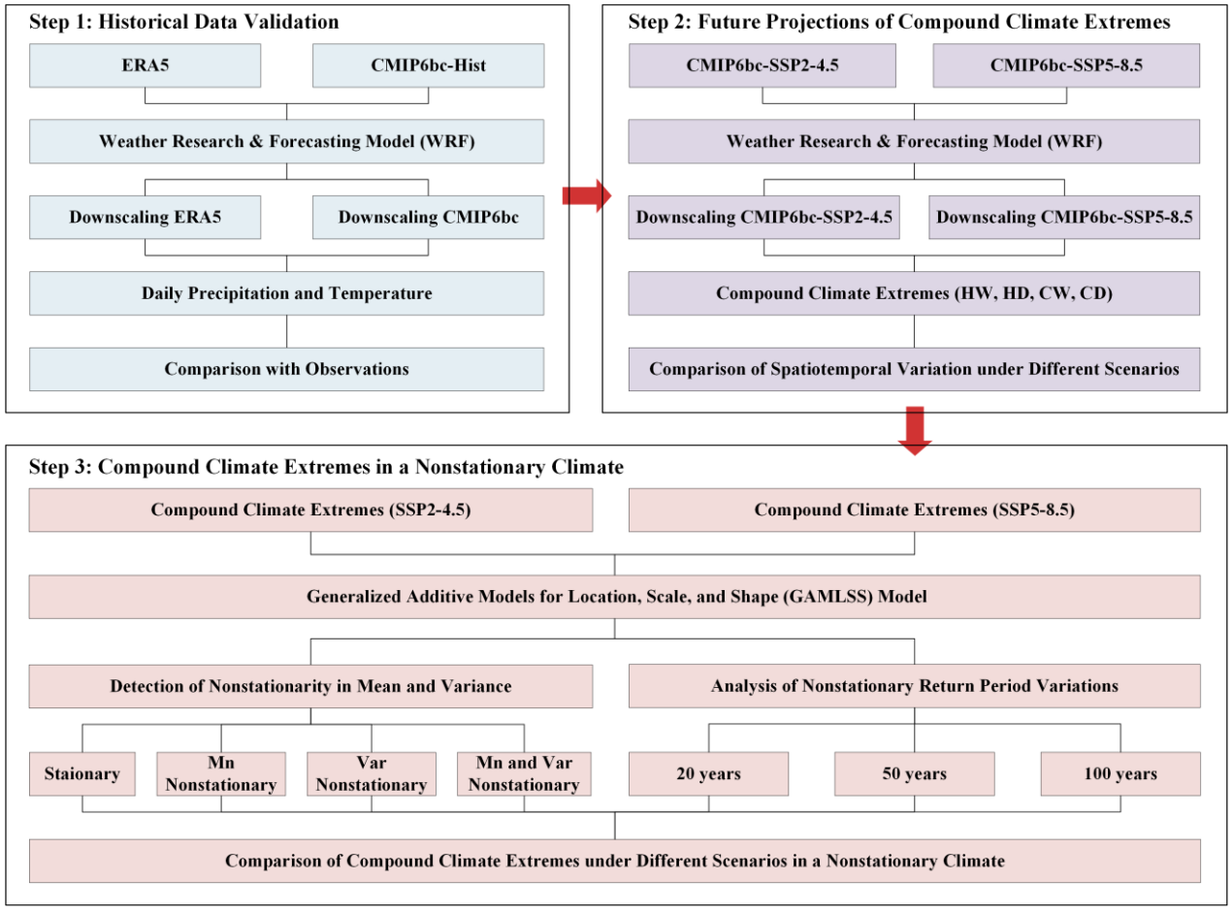

Figure 1. Flowchart of CCEs projection in a non-stationary framework.

2 Study region, methods and data

2.1 Study region

The MRB is a complex topographic basin in southeastern coastal China (Figure 2a). The Minjiang River, the main stream of the basin, drains an area of 60,992 km²–accounting for nearly half Fujian Province's territory. Encompassing three principal tributaries (Jianxi, Futunxi, and Shaxi rivers), the MRB experiences a subtropical monsoon climate characterized by 1700 mm mean annual precipitation and 18°C mean temperature. (Zheng et al., 2023). The basin displays spatio-temporal heterogeneity in precipitation, with flood seasons from April to September that often accompany CCEs. Particularly in the late flood season (July to September), the MRB experiences frequent typhoon-related compound disasters: the upper and middle reaches are commonly affected by typhoon-rainstorm-landslide events, while the lower reaches face high occurrences of typhoon-rainstorm-urban waterlogging and typhoon-rainstorm-flood events (Yang et al., 2025). In 2023, for

example, typhoon Doksuri (No. 2305) caused approximately 66,794 people to be affected in Fuzhou, the downstream city of the MRB, with direct economic losses reaching 588 million RMB (Yan et al., 2024). In addition, the region also exhibits a climate characteristic of concurrent rainfall and heat, with CCEs frequently occurring during the warm season, driven by high temperature and heavy rainfall (Sun et al., 2025).

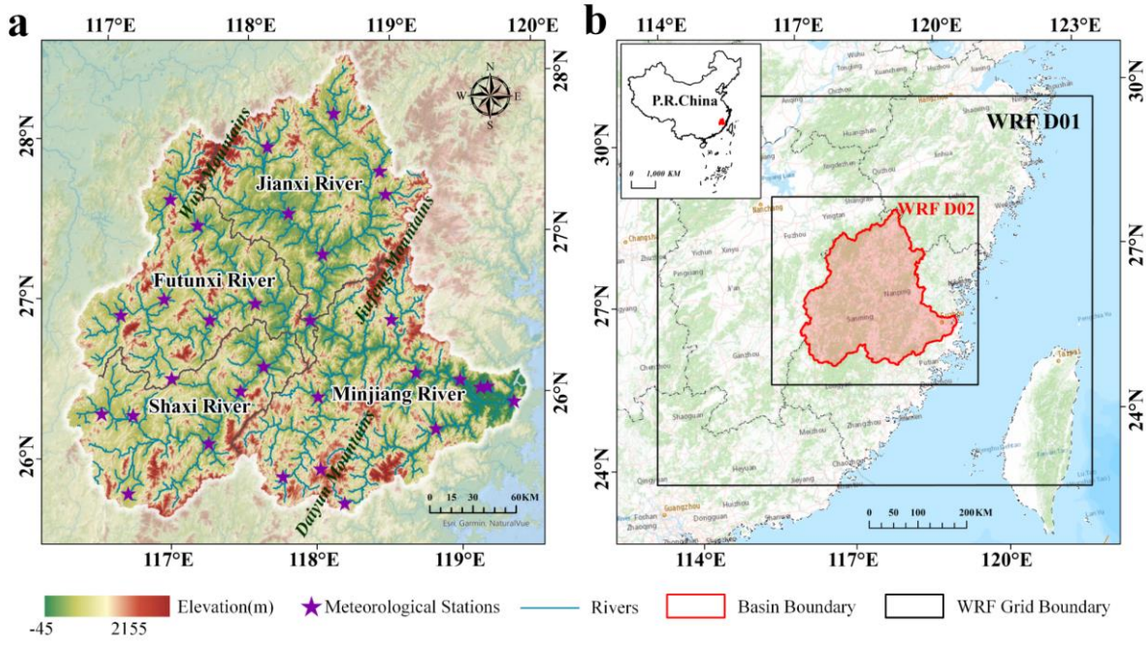

Figure 2. Study area and model configuration. (a) Topographic features of the MRB (m) and (b) Model configuration with 9-km (D01) and 3-km (D02) nested domains (Zhang et al., 2025). Basemap source: © Esri, https://services.arcgisonline.com

2.2 Data

Obtained from the Science Data Bank, the CMIP6bc dataset serves as the foundation for this investigation (Xu et al., 2021, https://www.scidb.cn), which is constructed using the ERA5. This dataset incorporates an 18-model CMIP6 ensemble mean (Supplement Table S1), maintaining both climatological mean and interannual variability statistics while preserving nonlinear temporal trends. Compared with original CMIP6 data, CMIP6bc demonstrates superior performance in extreme event simulation. Despite its widespread application in previous studies (Jamal et al., 2023; Huang et al., 2024; Wu and Zheng, 2023), we conduct a 10-year validation over the MRB. Considering both the reliability of the dataset and the need to optimize computational resources (simulating one year over the MRB requires approximately four days on 80 CPU cores), we select

a 10-year historical period (2005–2014) as sufficient to demonstrate the reliability of the CMIP6bc dataset for driving the WRF simulations. ERA5, as a widely used WRF-driven dataset (Arnault et al., 2021; Jiang et al., 2021; Varga and Breuer, 2022; Shang et al., 2022), is utilized here as a reference for the simulation results. Fujian Provincial Meteorological Bureau provides daily precipitation and temperature records from its 30 monitoring stations, which are used as validation data for this study. Future scenarios under SSP2-4.5 and SSP5-8.5 (2025–2065) are employed to project future changes in CCEs.

2.3 WRF model setup

This research utilizes the WRF Version 4.3 with two-domain nested configuration, featuring grid spacings of 9 km and 3 km (Figure 2b). Table 1 summarizes the optimal physics parameterization schemes selected through our comprehensive sensitivity experiments (Supplement Result S2) (Lin et al., 2023; Zhang et al., 2025). At sufficiently high model resolutions, deep convective processes can be explicitly resolved (Arakawa and Jung, 2011). Therefore, the cumulus parameterization scheme is deactivated in the inner domain (D02) to leverage convection-permitting capability. We first simulate daily precipitation and temperature over the MRB from January 1, 2005 to December 31, 2014, using both CMIP6bc and ERA5 forcing data. Subsequently, future projections from January 1, 2025 to December 31, 2065 are conducted using CMIP6bc under two climate projection scenarios.

Table 1 Settings for WRF model in this study.

WRF model setup overview		Parameterization scheme settings	
Forcing data	CMIP6bc, ERA5	Microphysics	Purdue Lin (Chen and Sun, 2002)
Centre	118.02E°, 26.83N°	Cumulus convection	New Tiedtke (Zhang et al., 2011)
Grid	100×90, 142×130	Longwave radiation	RRTMG (Mlawer et al., 1997)
Resolution	9km, 3km	Shortwave radiation	Dudhia (Dudhia, 1989)
E_vert	45	Boundary layer	YSU (Hong et al., 2006)
Spin-up time	7 days	Land surface	Noah-MP (Niu et al., 2011)

2.4 Definition of CCEs

This study considers four types of CCEs: hot-wet events (HW), hot-dry events (HD), cold-wet events (CW) and cold-dry events (CD). We adopt the widely used thresholds (the 90th and 10th percentiles) to identify CCEs (Croitoru et al., 2016; Song et al., 2019; Patel et al., 2024). We first extract daily precipitation (>0.1 mm) and temperature data for each grid during 2025-2065, defining

the 90th and 10th percentiles as thresholds to identify hot/cold and wet/dry extremes, respectively. Specifically, we define extreme temperature events as occurring when daily temperatures are higher (hot extremes) or lower (cold extremes) than the threshold. Wet events are characterized by rainfall surpassing the threshold (90th), while dry events are characterized by seven consecutive days without rainfall. We conduct calculations independently for each grid point, applying thresholds specific to each point. Specifically, for interannual variation, we sort the precipitation and temperature data over a 40-year period and determine the thresholds based on the 10th and 90th percentiles to identify CCEs. For seasonal variations, we separately extract the precipitation and temperature data for the summer (JJA) and winter (DJF) seasons, applying the same sorting method to calculate the respective thresholds, thus analyzing the distribution characteristics of CCEs for each season.

2.5 GAMLSS model

GAMLSS is a flexible statistical model used for analyzing distributions with non-stationary characteristics (Rigby and Stasinopoulos, 2005). It extends the traditional generalized linear models (GLMs) and generalized additive models (GAMs) by introducing joint modeling of all distribution parameters (location, scale, and shape). Unlike traditional regression models, GAMLSS effectively characterizes both linear and nonlinear dependencies linking predictors to response variables. (D. M. Stasinopoulos and Rigby, 2007).

This study employs the semi-parametric GAMLSS, which accommodates parametric terms, nonparametric smooth functions, and random effects within a unified modeling structure (Gao et al., 2018). Consider z independent samples $y_i(i = 1, \dots, z)$ following a distribution $F_y(y_i\theta_i)$, where the parameter vector $\theta_{iT} = (\theta_{i1}, \theta_{i2}, \dots, \theta_{ik})$ contains k components representing location (Mn), scale (Var), and shape (skewness and kurtosis), with k normally not exceeding 4. Model selection is performed using Akaike's Information Criterion (AIC) (Akaike, 1974), with the optimal configuration identified through minimum AIC values., and model fitting quality is assessed by the Filliben correlation coefficient (Filliben, 1975). The GAMLSS is formally defined as follows:

$$g_k(\theta_k) = \emptyset_k\beta_k + \sum_{j=1}^{j_k} h_{j_k}(x_{j_k})$$

where k denotes the indicator of distribution parameters, θ_k is the distribution parameter vector, $\emptyset_k$ represents $n \times j_k$ matrix of covariate variables, β_k is the coefficient vector of length j_k. $g_k(\cdot)$ is the link function connecting distribution parameter to linear predictor. $h_{j_k}(\cdot)$ defines how the distribution parameter varies with covariate variable x_{j_k}. In the GAMLSS model, time (year) is used as the independent variable (x), and the number of days per year for each type of CCE is treated as the dependent variable (y), thereby enabling the calculation of the non-stationary characteristics of each CCE. We employ two types of GAMLSS models to capture potential changes in the distribution of meteorological variables. The first is the traditional two-parameter location–scale model (mean μ and variance σ), which assumes a fixed distributional shape. The second is a more flexible four-parameter location–scale–shape model (mean μ, variance σ, skewness ν, and kurtosis τ), allowing the distributional shape to evolve over time. These extended models retain the mean and variance parameters while incorporating two additional shape parameters to capture asymmetry and tail behavior. We assess the models by comparing their goodness of fit and select the one that best represents the data distribution for subsequent analyses. Regarding the calculation of stationarity, we consider the CCEs to be stationary if both the mean and variance remain stable. If either the mean or variance shows significant variation, the CCEs are considered non-stationary. Supplement Table S2 lists all the distribution functions implemented in our study. The R code for implementing GAMLSS model can be accessed at https://github.com/gamlss-dev/gamlss.

3 Results

3.1 Spatio-temporal patterns of CCEs under future scenarios

Figures 3 (a–j) illustrate the spatial distribution of annual CCEs over the MRB during 2025–2065. Overall, total CCEs are higher under the SSP5-8.5 scenario (45.48 days) than under the SSP2-4.5 scenario (42.58 days). Dry-related extremes (HD and CD) dominate across the basin, whereas wet-related extremes (HW and CW) are less frequent. Both hot extremes occur more frequently under SSP5-8.5 than SSP2-4.5: HW increases from 0.84 to 1.33 days, and HD rises from 22.69 to 27.45 days. In contrast, cold extremes decrease: CW declines from 3.17 to 2.15 days, and CD from 15.88 to 14.19 days.

Spatially, the two scenarios exhibit similar geographic patterns. The highest frequencies occurring in downstream regions, particularly for HD and HW. HD shows a wider spatial extent,

extending into the Futun River and Jian River Basins. Meanwhile, CW and CD display a clear west-to-east increasing gradient, with the highest values concentrated near the Jiufeng Mountains.

Temporally (Figures 3 k–o), CCE trends diverge sharply between scenarios. Under high-emission SSP5-8.5, total CCEs increase significantly at 3.55 days per decade, whereas SSP2-4.5 projects stabilized frequencies. Hot extremes (HW and HD) increase more rapidly under SSP5-8.5, at rates nearly double those under SSP2-4.5. Conversely, the decline in CD is stronger under SSP2-4.5— approximately 1.7 times that under SSP5-8.5.

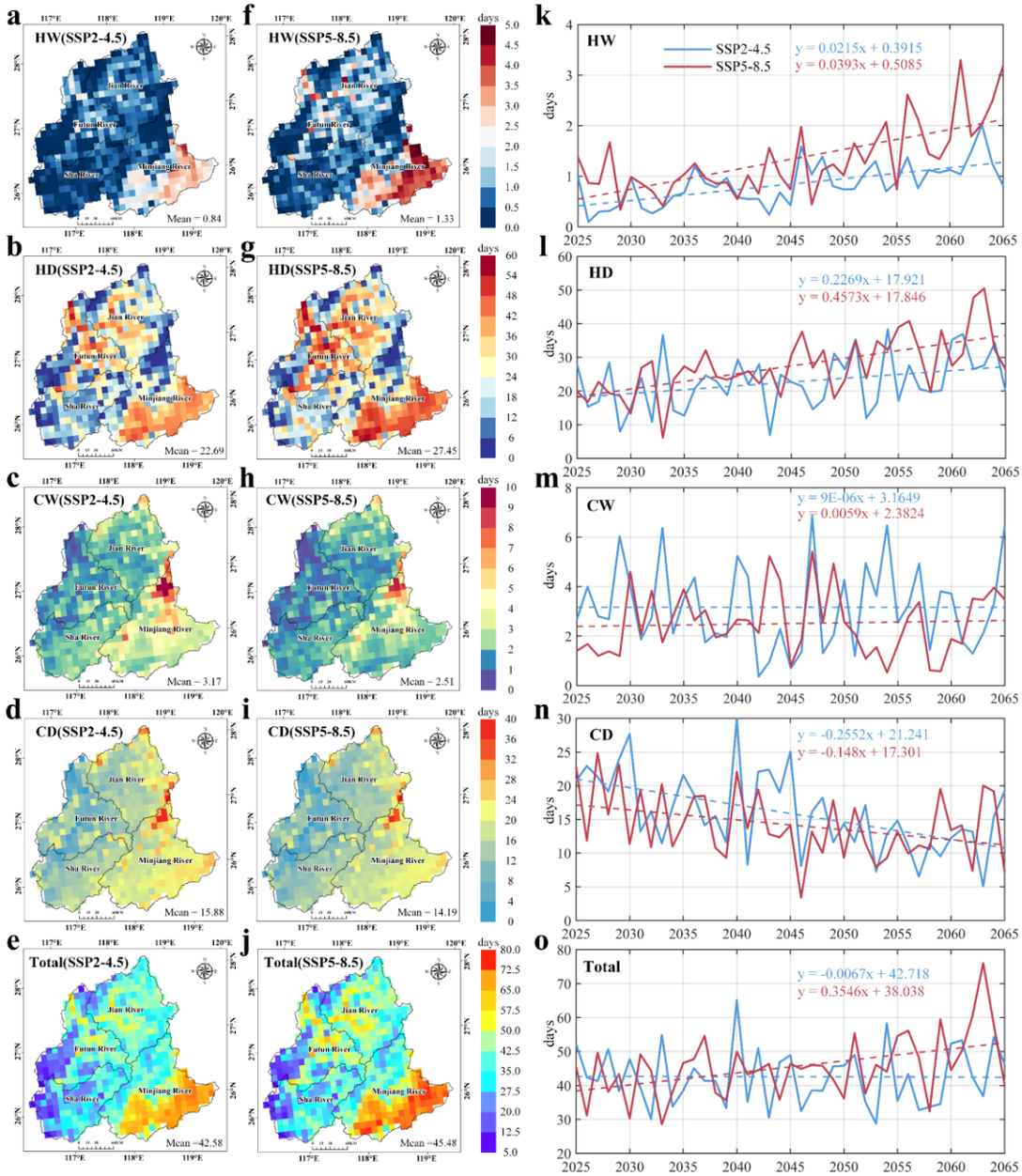

Figure 3. Annual Spatio-temporal patterns of CCEs across the MRB from 2025 to 2065.

Building on the analysis of annual changes, we further investigate the seasonal variations of CCEs. As shown in Figures 4 (a–j), the spatial distribution of summer CCEs largely resembles the annual pattern, except for HW, which remain infrequent in this season. Nonetheless, a marked increase in HW under the SSP5-8.5 is observed in the downstream MRB. In summary, total CCEs increase during summer under both scenarios, rising more rapidly under SSP5-8.5 (2.26 days per decade) than under SSP2-4.5 (0.79 days per decade). Moreover, differences between scenarios are more pronounced for hot-related extremes (HW and HD) in summer than on the annual scale, whereas cold-related events (CW, CD) show consistent patterns (Figures 5 a–e).

In winter, CCEs exhibit a contrasting spatial distribution (Figures 4 k–t). They occur predominantly in the western MRB, particularly concentrated in the Futun River Basin, with higher frequencies under SSP5-8.5 (11.87 days) than under SSP2-4.5 (11.51 days). This shift is primarily driven by hot-related extremes (HW and HD), which move from the downstream MRB toward western mountainous areas. Meanwhile, cold-related extremes (CW and CD) remain most frequent in the Jiufeng Mountain areas. Winter CCEs show an increasing trend under SSP5-8.5 (0.76 days per decade) but a slight decreasing trend under SSP2-4.5 (Figures 5 f–j). Among individual event types, wet-related extremes (CW and HW) show insignificant trends, whereas HD increases (1.18 and 0.46 days per decade under SSP5-8.5 and SSP2-4.5, respectively) and CD deceases (–0.50 and –0.70 days per decade under the two scenarios).

Given the importance of precipitation and temperature as key climate indicators, we calculate their basin-averaged annual values and interannual trends. (Supplement Figure S5). Precipitation varies only slightly, maintaining relatively stable annual fluctuations. In contrast, temperature shows a distinct upward trend, which accelerates under high-emission SSP5-8.5 conditions (0.46°C per decade). These results suggest that changes in CCEs across the MRB are primarily governed by temperature-driven physical processes — where intensifying hot extremes coincide with declining cold extremes—a conclusion supported by earlier studies (Wu et al., 2020; Zhao et al., 2024; Duan et al., 2024).

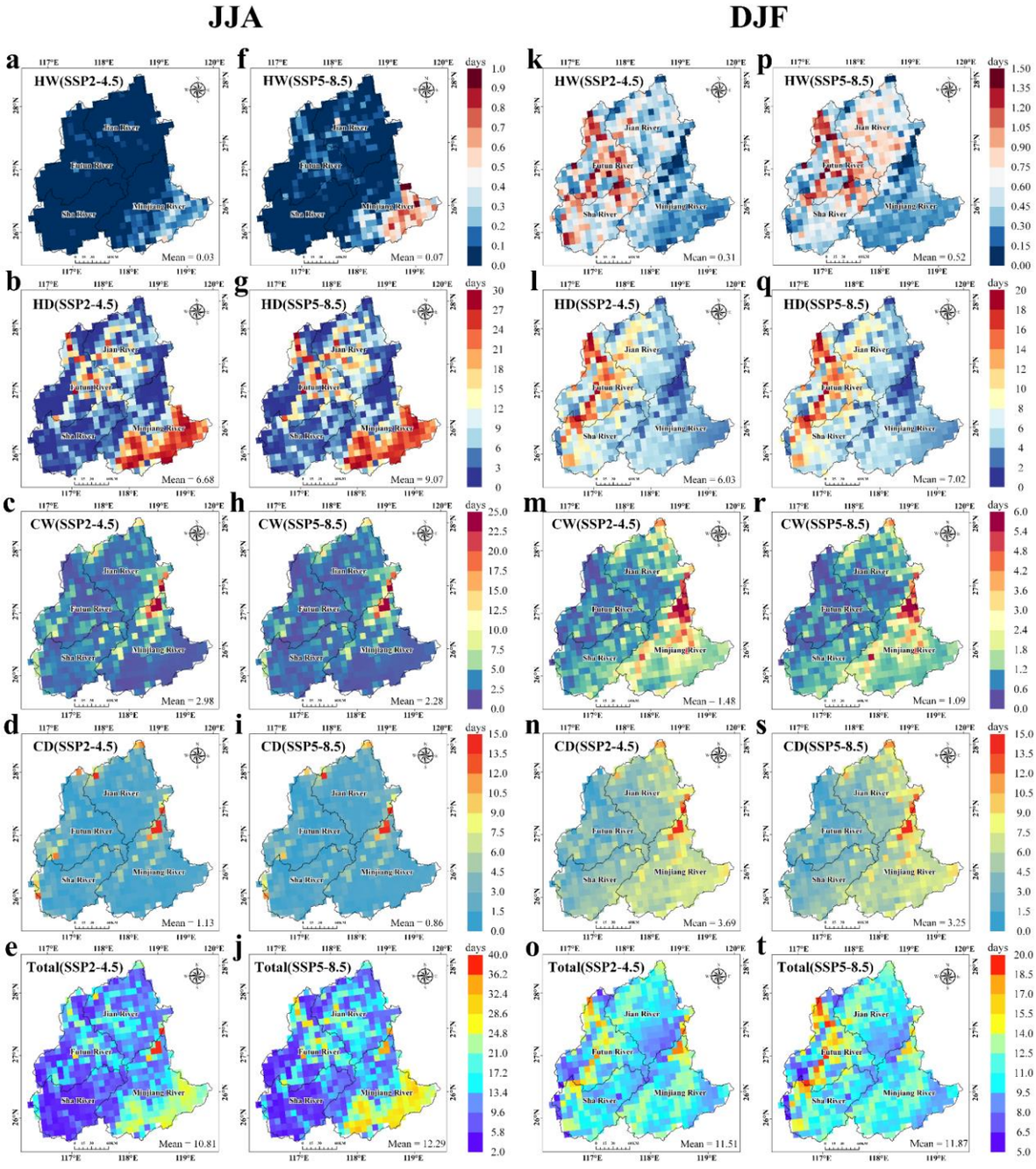

Figure 4. Spatial patterns of CCEs in summer (JJA) and winter (DJF) across the MRB from 2025 to 2065.

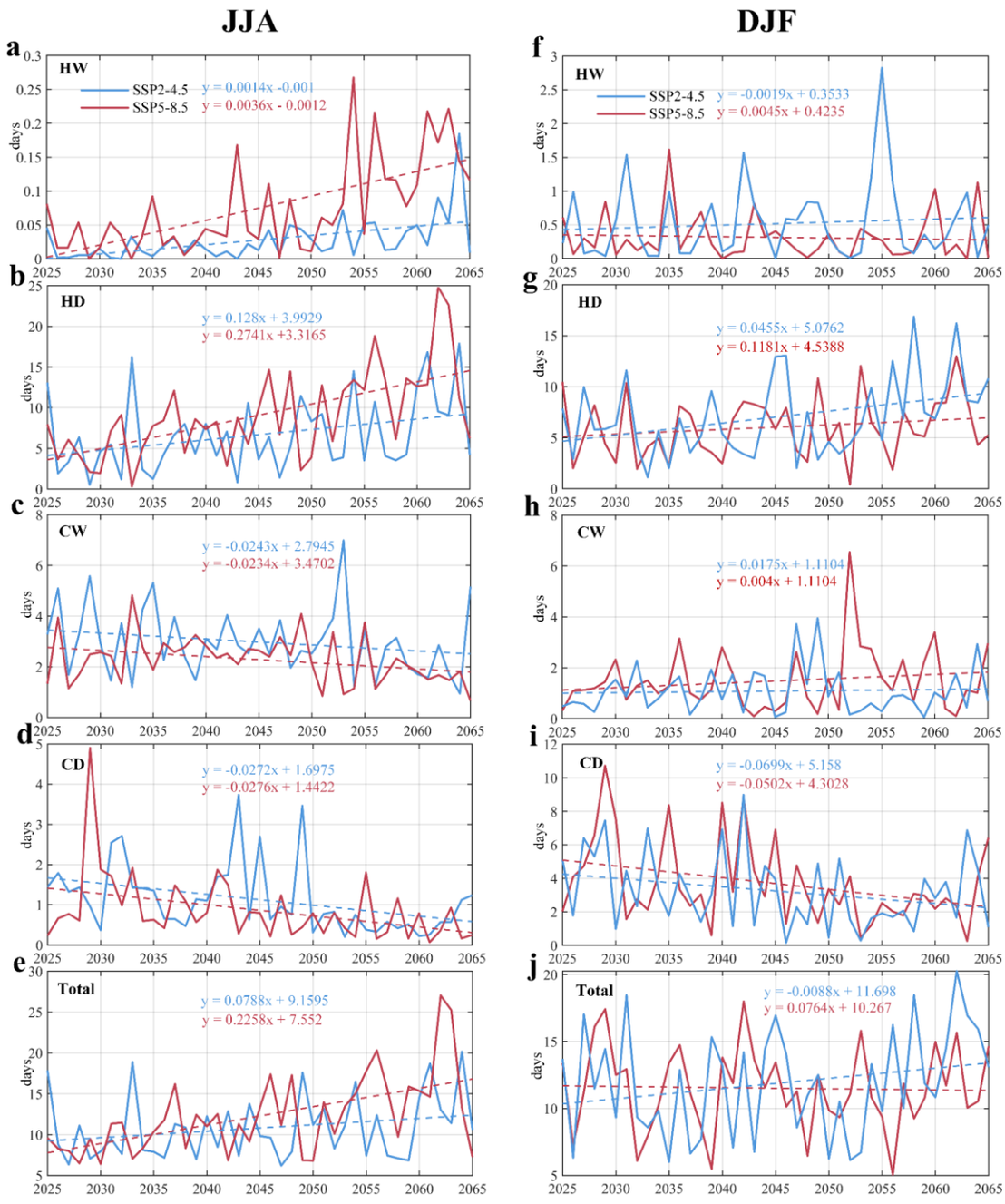

Figure 5. Temporal patterns of CCEs in summer (JJA) and winter (DJF) across the MRB from 2025 to 2065.

3.2 Non-stationary characteristics of CCEs

To quantify the non-stationary characteristics of CCEs, we analyze variations in both the mean (Mn) and variance (Var) using GAMLSS (Figure 6). The model demonstrates excellent fitting performance for all indices except HW, as indicated by Filliben coefficients exceeding 0.95 in Supplement Figure S6.

Our results reveal a pronounced shift from stationary to non-stationary behavior in CCEs under SSP5-8.5 compared to SSP2-4.5. This shift is primarily driven by non-stationarity in Mn, which governs 80.81% of grid cells across the MRB. An additional 11.07% of grids are influenced by the combined effects of both Mn and Var, primarily distributed in the Shaxi River Basin and the downstream MRB. Dry-related extremes (HD and CD) show a transition from Var to Mn non-stationarity. For HD, the area dominated by Mn non-stationarity expands from 22.65% to 57.03% of grids, becoming the prevailing pattern (covering 60% of grids) in downstream regions where stationarity was previously dominant (54.71%). Similarly, Mn non-stationarity for CD expands to cover nearly the entire downstream MRB. For wet-related extremes (HW and CW), both Mn and Var non-stationarity increase notably. The area dominated by Mn non-stationarity for HW rises from 34.30% to 54.02% of grids, while for CW, it undergoes a more substantial increase from 0.06% to 23.25%. Overall, CCEs under SSP5-8.5 display more widespread non-stationarity, with dry-related extremes primarily governed by changes in Mn, whereas wet extremes are influenced by a combination of Mn and Var effects.

Figure 7 further details the spatial patterns of Mn and Var in CCEs. Compared to Var, Mn exhibits more pronounced and spatially extensive variations. For hot-related extremes (HW and HD), Mn increases significantly across the entire basin under both SSP2-4.5 and SSP5-8.5 (at the 99% confidence level), indicating that climate warming predominantly amplifies the mean frequency of hot-related extremes rather than their temporal variability. For cold-related extremes, CD exhibits more stronger changes than CW, which are also predominantly driven by reduction in Mn. Under SSP5-8.5, Mn for most CCEs increases significantly across nearly the entire basin, while under SSP2-4.5, it remains relatively stable. In contrast, Var exhibits only minimal changes under both scenarios.

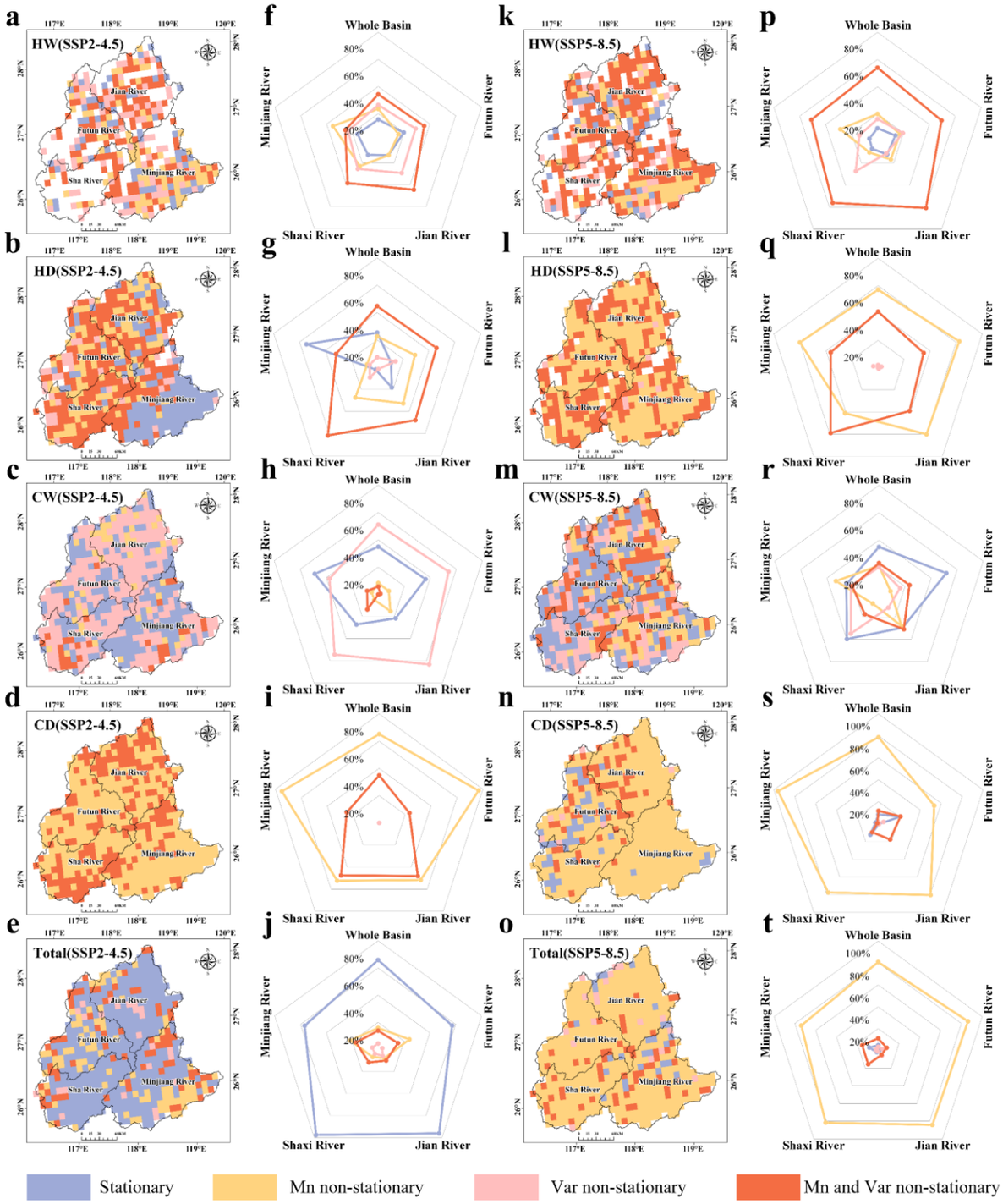

Figure 6. Stationary and non-stationary characteristics for CCEs in the MRB (a-e and k-o), percentage of non-stationary and stationary characteristics across five basins (f-j and p-t).

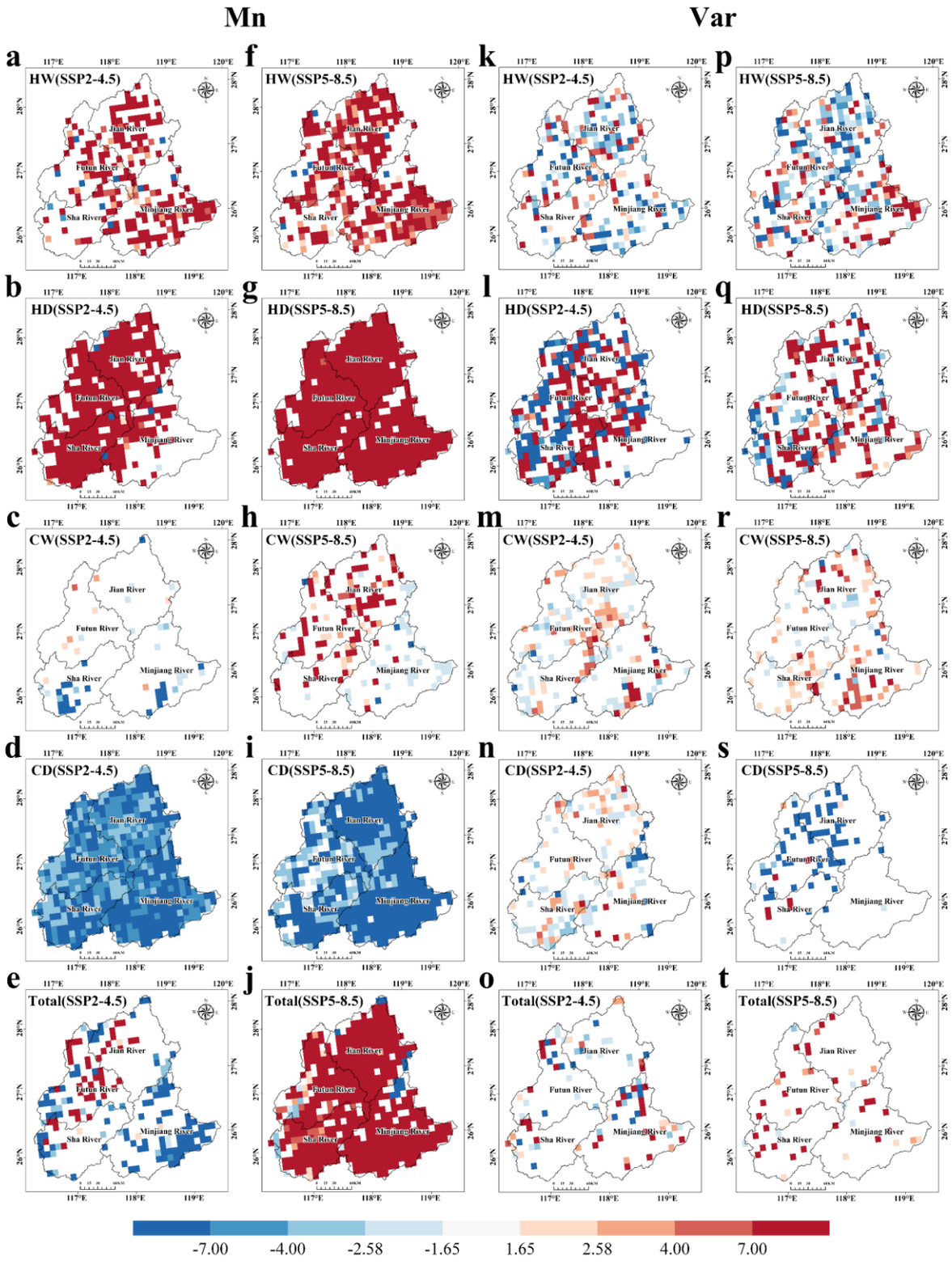

Figure 7. Results of Mann-Kendall test for Mn (a-j) and Var (k-t), showing the spatial distribution of Z values. Z values indicate trend significance: $|Z| > 1.65$ denotes 90% confidence, while $|Z| > 2.58$ corresponds to 99% confidence.

3.3 Changes in the recurrence frequency of CCEs

To assess changes in the recurrence frequency of CCEs, we fit both stationary and non-stationary models. As shown in Figures 8 (a-j), substantial differences emerge between the return periods estimated under stationary versus non-stationary assumptions. Our results reveal that stationary models systematically underestimate the future recurrence frequency of CCEs, whereas non-stationary models reasonably capture their time-evolving characteristics. This underestimation gap widens notably over time.

Under SSP5-8.5, non-stationary projections indicate significant increases in the frequency of CCEs corresponding to 20-, 50-, and 100-year return periods. For instance, total CCEs with a 100-year return period are projected to increase at a rate of 3.12 days per decade. Stationary models consistently underestimate CEE frequency after around 2045. Specifically, HW, HD, and CW all show positive trends in recurrence frequency under SSP5-8.5 with increases of 0.36, 11.65, and 0.30 days per decade, respectively. Under SSP2-4.5, the corresponding increases are lower (0.15, 2.53, and 0.06 days per decade). In contrast, CD exhibits a decreasing trend, with a more rapid decline under the SSP2-4.5 (-3.38 days per decade) than under SSP5-8.5. The 100-year return events display greater sensitivity to climate change, highlighting amplified non-stationary effects on these high-impact extremes.

We further quantify the deterministic trends in recurrence frequency using Empirical Mode Decomposition (EMD, Supplement Method S1). Figures 8 k-t present the variations in the 100-year recurrence frequency (complete results for all return periods are provided in Supplementary Figure S7). Overall, CCE frequency shows strong upward trends under SSP5-8.5, with significant spatial heterogeneity. Frequency generally decreases from west to east, with notably high-value areas concentrated in the Shaxi River Basin (exceeding 12 days per decade in some grids). Among all indices, HD exhibits the most severe increase, with basin-wide trends exceeding 8 days per decade. CD is the only index showing a decreasing trend under both scenarios, with a less pronounced decline under SSP5-8.5, suggesting that greenhouse warming has only partially offset the reduction in CD recurrence frequency.

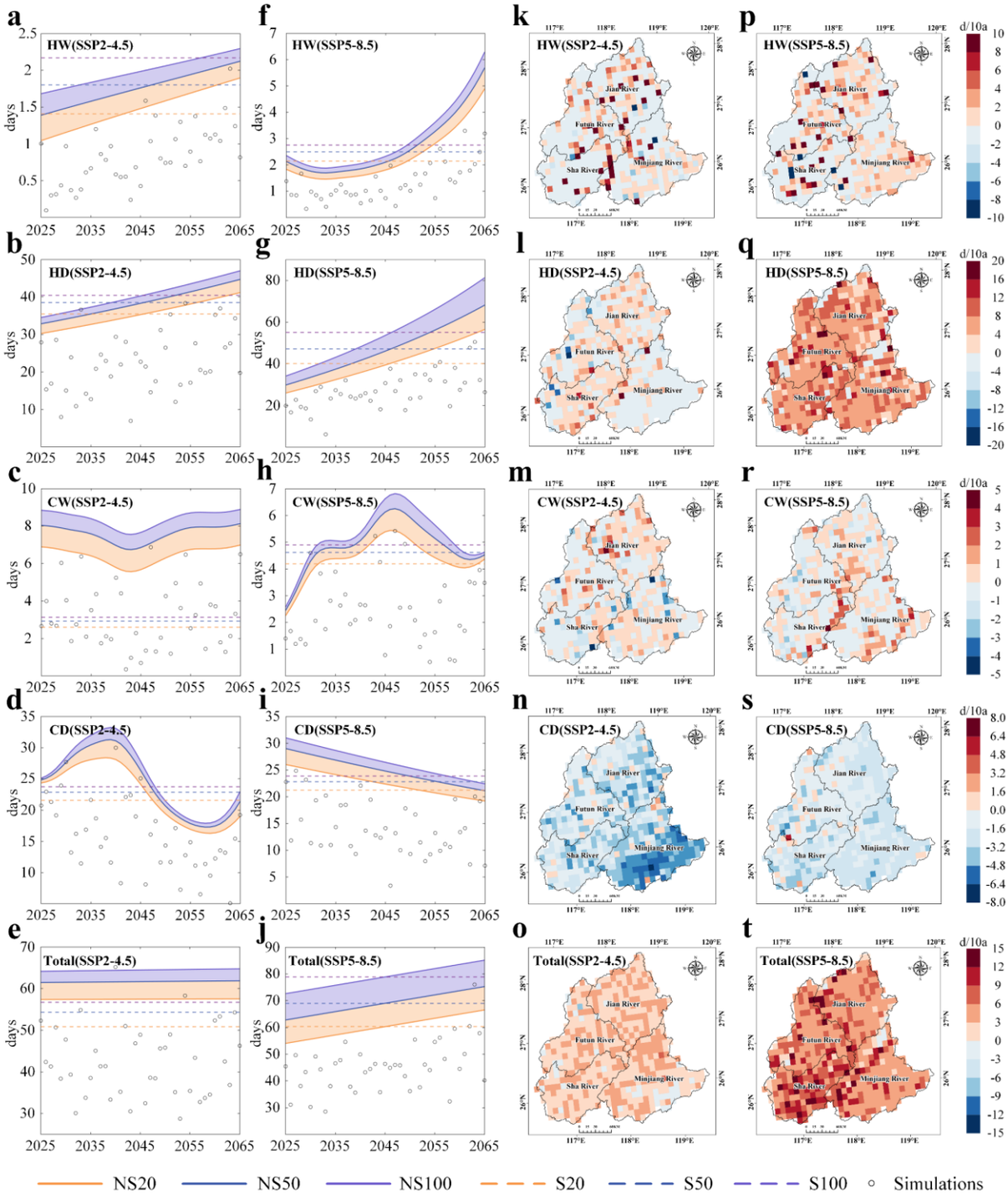

Figure 8. Comparison of non-stationary (NS) and stationary (S) characteristics for CCEs under 20-, 50-, and 100- year return periods (a-j). Spatial distributions of trends in CCEs under 100-year return periods (k-t), 20- and 50-year return period result are provided in Supplement Figure S7.

4 Discussion

Although earlier research has emphasized the necessity of analyzing extreme events under non-stationary conditions (Cheng et al, 2014; Byun and Hamlet, 2020; Liu et al., 2024), the evolution of CCEs within a non-stationary climate remains lacking. Our study develops an innovative non-stationary framework integrating WRF-based dynamical downscaling with GAMLSS to reassess future recurrence frequency of CCEs. The results indicate that traditional stationary models systematically underestimate the frequency of CCEs, highlighting the critical importance of incorporating time-varying risk assessments to avoid misleading projections and to inform robust climate adaptation strategies (Abdelmoaty and Papalexiou, 2023). This innovative framework enables regional-scale reassessment of CCEs which is transferable to other regions.

4.1 Dominance of hot extremes and temperature-driven shifts

The projected increase in CCEs, particularly under SSP5-8.5, aligns with global trends of intensifying hydroclimatic risks under continued warming (Asadieh and Krakauer, 2017; Zhang et al., 2021; Shu et al., 2024). Our findings indicate that hot-dry extremes dominate both spatially and temporally, increasing at 2.26 days per decade in summer under SSP5-8.5, while cold extremes decline. This pattern is consistent with studies highlighting the rising prevalence of hot-stagnation and hot-dry extremes in East Asia (Yin et al., 2025). The reversal between hot and cold extremes has been robustly linked to enhanced radiative forcing from anthropogenic greenhouse gas emissions (Samset et al., 2018; Kramer et al., 2021). Our analysis further reveals that temperature—not precipitation—is the primary driver of CCE changes in the MRB, as evidenced by the strong warming trend (0.46°C per decade under SSP5-8.5) alongside relatively stable precipitation (Supplement Figure S5). This supports the hypothesis that thermodynamic effects, rather than dynamic ones, dominate mean-state changes in extremes (Horton et al., 2016; Van Der Wiel and Bintanja, 2021).

4.2 Non-stationarity: mean shifts outpace variability

A key advance of this study is the explicit detection of non-stationary characteristics in CCEs, which has been largely overlooked in prior compound event analyses. We find that under SSP5-8.5, 95.20% of grid cells exhibit non-stationarity, predominantly driven by changes in the Mn rather than Var, accounting for 80.81% of the transitions. This suggests that climate warming amplifies

383 extremes primarily through shifts in baseline intensity—a thermodynamic effect—rather than
384 through increased temporal variability. Similar findings have been reported at global scales, where
385 mean warming dominates changes in extreme temperature distributions (Patel et al., 2024; Nordling
386 et al., 2025). The spatial concentration of Mn-driven non-stationarity in downstream MRB and the
387 Shaxi River Basin may reflect localized warming amplification due to urban heat islands or land-
388 atmosphere feedbacks, a phenomenon noted in other subtropical regions (Gao et al., 2018; Wu et
389 al., 2020).

390 **4.3 Frequency of recurrence systematically underestimated by stationary model**

391 Our comparison between stationary and non-stationary model indicates that the latter captures a
392 significant increase in recurrence risks, particularly for 100-year CCEs, which are projected to rise
393 by 3.12 days per decade under the SSP5-8.5 scenario. Stationary model systematically
394 underestimates recurrence frequency after 2045, and the stronger non-stationary response of 100-
395 year events highlights the heightened vulnerability of high-impact, low-probability extremes.
396 Additionally, the west-to-east gradient in recurrence frequency, with hotspots in the Shaxi River
397 Basin, may be attributed to topographic and land-surface heterogeneity, which modulate local
398 hydroclimatic responses (Zheng et al., 2023). Previous studies have similarly shown that
399 conventional extreme value models fail to capture the escalating severity of extreme events under
400 climate change. Singh et al. (2021) demonstrated that under climate change, precipitation and
401 temperature exhibit a non-stationary dependent structure, and treating them independently can
402 substantially underestimate the occurrence of compound extremes. Feng et al. (2020) compared the
403 recurrence probabilities of floods under stationary and non-stationary conditions and found that,
404 under non-stationary conditions, the annual variability of floods is significantly greater. Xu et al.
405 (2025) evaluated changes in global marine heatwaves and found that stationary models significantly
406 underestimate their frequency, intensity, and duration. In summary, these studies collectively
407 highlight that accounting for non-stationarity is crucial for accurately assessing various extreme
408 events.

409 **4.4 Methodological limitations**

410 Our integrated 'bias-corrected CMIP6–WRF dynamical downscaling–GAMLSS' framework
411 represents a significant methodological advancement over the direct use of purely statistical

downscaling for projecting CCEs. By resolving mesoscale circulations and explicitly simulating convective processes, our approach more faithfully captures the fine-scale spatiotemporal heterogeneity of precipitation and temperature fields in complex terrain, a capability that statistical methods, reliant on historically derived statistical relationships, fundamentally lack (Gutmann et al., 2012; Rahimi et al., 2024). Nevertheless, certain limitations persist. Even at convection-permitting resolution (3 km), the WRF model exhibits systematic biases in simulating orographic precipitation, a well-documented challenge often stemming from uncertainties in microphysical parameterization schemes and the representation of land-atmosphere energy and moisture exchanges over mountainous regions (Talbot et al., 2012; Zhang et al., 2025). Furthermore, while statistically robust, our current non-stationary GAMLSS framework employs time merely as a proxy covariate for climate change. This approach effectively detects and projects temporal trends in risk but falls short of elucidating the underlying physical drivers, such as the specific roles of evolving large-scale circulation patterns or soil moisture-atmosphere feedbacks. To overcome these constraints and solidify the physical foundations of our projections, future work should focus on three promising avenues: first, explicitly embedding physical drivers like atmospheric circulation indices, antecedent soil moisture, or global mean temperature as covariates within the GAMLSS to establish a clearer causal chain from forcing to statistical response (Zeng et al., 2024; Ma et al., 2025); second, leveraging machine learning, such as convolutional neural networks, for the statistical post-processing of WRF outputs to correct systematic biases, or developing hybrid physics-informed machine learning models as a complementary approach to dynamical downscaling (Yin et al., 2021; Xie et al., 2023); and third, employ multi-RCMs ensemble forecasts to comprehensively address and minimize the uncertainties inherent in the downscaling process, thereby enhancing the robustness and reliability.

5 Conclusions

Through this intensive case analysis, we establish a transferable framework for assessing the non-stationarity of CCEs. This work advances the understanding of the evolution of CCE recurrence frequency under climate change and offers important perspectives to support adaptive strategies and strengthen disaster risk governance. The main findings are summarized as follows:

1) CCEs increase significantly across the MRB, with a stronger trend under SSP5-8.5 (3.55 days

per decade) than under SSP2-4.5. HD extremes dominate both spatially (downstream-focused) and seasonally (summer-peaked), rising at 2.26 days per decade, whereas cold extremes decline. These shifts are primarily temperature-driven, as pronounced warming amplifies hot-related extremes but suppresses cold-related extremes.

2) CCEs shift markedly toward Mn-dominated non-stationarity under SSP5-8.5 scenarios, contrasting with the largely stationarity under SSP2-4.5. Spatially, Mn non-stationarity governs 80.8 % of the MRB under SSP5-8.5, with dry-related extremes (HD and CD) showing the most abrupt transitions. For HD, Mn non-stationarity expands from 22.7% to 57.0% of the basin and dominates 60% of downstream grids—an increase of nearly threefold relative to SSP2-4.5. For CD, Mn-driven shifts cover >90% of the downstream MRB. Var contributes minimally in both scenarios, confirming that warming amplifies extremes primarily through shifts in mean intensity rather than through increased variability.

3) Non-stationary modeling reveals that stationary approaches systematically underestimate future CCEs recurrence frequency. Under SSP5-8.5, most CCEs types (except CD) exhibit increasing recurrence frequency. Climate change impacts are significantly amplified for 100-year return period events, which rise at 3.12 days per decade—a response highlighting their heightened non-stationary sensitivity. Spatially, recurrence frequency shows a distinct east-to-west gradient, with a significantly increase occurring in the western mountainous areas.

Acknowledgements

The 'High Performance Computing Center' at Fujian Normal University provided computational resources for the WRF model simulations.

Financial support

Supported by the National Natural Science Foundation of China (Grant No. 42271030), Fujian Provincial Funds for Distinguished Young Scientists (Grant No. 2022J06018), the Scientific Project of Fujian Provincial Department of Science and Technology (Grant no. 2022Y0007), the German Federal Ministry of Education and Research (BMBF) through funding of the KARE_II project (01LR2006D1) and the 'Young Eagle Plan' Top Talents of Fujian Province. Lu Gao is financially supported by the Humboldt Research Fellowship for Experienced Researchers through Alexander von Humboldt Foundation. Yinchi Zhang gratefully acknowledge financial support from the China Scholarship Council (CSC).

Code/Data availability

Code/Data will be made available on request.

Declaration of competing interest

The authors declare that they have no known competing financial interests or personal relationships that could have appeared to influence the work reported in this paper.

Author contribution

Conceptualization: YZ. Methodology: YZ, LG, WX, CD, MM, JW, HK. Software: YZ, WX, CD. Data curation: SS. Writing- Original draft preparation: YZ. Writing- Reviewing and Editing: WX, YW, LG. Supervision: SS, MM, YC, HK. Funding acquisition: LG, JW, YC.

References

Abdelmoaty, H.M., Papalexiou, S.M., 2023. Changes of extreme precipitation in CMIP6 projections: should we use stationary or nonstationary models? J. Climate 36, 2999–3014. https://doi.org/10.1175/JCLI-D-22-0467.1

Akaike, H., 1974. A new look at the statistical model identification. IEEE T. Automat. Contr. 19(6), 716–723. https://doi.org/10.1109/TAC.1974.1100705

Arakawa, A., Jung, J.-H., 2011. Multiscale modeling of the moist-convective atmosphere — A review. Atmos. Res. 102, 263–285. https://doi.org/10.1016/j.atmosres.2011.08.009

Arnault, J., Jung, G., Haese, B., Fersch, B., Rummler, T., Wei, J., Zhang, Z., Kunstmann, H., 2021. A joint soil - vegetation - atmospheric modeling procedure of water isotopologues: implementation and application to different climate zones with WRF - Hydro - iso. J. Adv. Model Earth Syst. 13. https://doi.org/10.1029/2021MS002562

Asadieh, B., Krakauer, N.Y., 2017. Global change in streamflow extremes under climate change over the 21st century. Hydrol. Earth Syst. Sci. 21, 5863–5874. https://doi.org/10.5194/hess-21-5863-2017

Byun, K., Hamlet, A.F., 2020. A risk-based analytical framework for quantifying non-stationary flood risks and establishing infrastructure design standards in a changing environment. J. Hydrol. 584, 124575. https://doi.org/10.1016/j.jhydrol.2020.124575

Byun, U., Chang, E., Kim, J., Ahn, J., Cha, D., Min, S., Byun, Y., 2023. Investigation of Added Value in Regional Climate Models for East Asian Storm Track Analysis. J. Geophys. Res.: Atmos. 128, e2023JD039167. https://doi.org/10.1029/2023JD039167

Chen, G., Mei, S.-J., Hang, J., Li, Q., Wang, X., 2025. URANS simulations of urban microclimates: Validated by scaled outdoor experiments. Building and Environment 272, 112691. https://doi.org/10.1016/j.buildenv.2025.112691

Chen, S.-H., Sun, W.-Y., 2002. A one-dimensional time dependent cloud model. J. Meteorol. Soc. Japan. 80, 99–118. https://doi.org/10.2151/jmsj.80.99

Cheng, L., AghaKouchak, A., Gilleland, E., Katz, R.W., 2014. Non-stationary extreme value analysis in a changing climate. Climatic Change 127, 353–369. https://doi.org/10.1007/s10584-014-1254-5

509 Croitoru, A.-E., Piticar, A., Ciupertea, A.-F., Roşca, C.F., 2016. Changes in heat waves indices in
510 Romania over the period 1961–2015. Global and Planetary Change 146, 109–121.
511 https://doi.org/10.1016/j.gloplacha.2016.08.016
512 Duan, R., Huang, G., Wang, F., Tian, C., Wu, X., 2024. Observations over a century underscore an
513 increasing likelihood of compound dry - hot events in China. Earth's Future 12,
514 e2024EF004546. https://doi.org/10.1029/2024EF004546
515 Dudhia, J., 1989. Numerical Study of Convection Observed during the Winter Monsoon
516 Experiment Using a Mesoscale Two-Dimensional Model. J. Atmos. Sci. 46, 3077–3107.
517 https://doi.org/10.1175/1520-0469(1989)046<3077:NSOCOD>2.0.CO;2
518 Fang, P., Wang, T., Yang, D., Tang, L., Yang, Y., 2025. Substantial increases in compound climate
519 extremes and associated socio-economic exposure across China under future climate change.
520 npj Clim. Atmos. Sci. 8, 17. https://doi.org/10.1038/s41612-025-00910-7
521 Feng, Y., Shi, P., Qu, S., Mou, S., Chen, C., Dong, F., 2020. Nonstationary flood coincidence risk
522 analysis using time-varying copula functions. Sci. Rep. 10, 3395.
523 https://doi.org/10.1038/s41598-020-60264-3
524 Filliben, J.J., 1975. The probability plot correlation coefficient test for normality. Technometrics 17,
525 111–117. https://doi.org/10.1080/00401706.1975.10489279
526 Gan, B., Liu, M., Cui, H., Chen, X., Chen, Y., Gao, L., Deng, H., 2025. Spatiotemporal patterns and
527 propagation of meteorological and hydrological drought in a humid basin of Southeast China.
528 Sci. Rep. 15, 31720. https://doi.org/10.1038/s41598-025-17005-1
529 Gao, L., Huang, J., Chen, X., Chen, Y., Liu, M., 2018. Contributions of natural climate changes and
530 human activities to the trend of extreme precipitation. Atmos. Res. 205, 60–69.
531 https://doi.org/10.1016/j.atmosres.2018.02.006
532 Geng, K., Chen, X., Zheng, M., Gao, Y., Gu, Z., Yao, H., 2024. The influence of human activities
533 on rainfall-runoff relationships at different time scales in the Minjiang River Basin. Theor.
534 Appl. Climatol. 155, 8435–8454. https://doi.org/10.1007/s00704-024-05124-0
535 Gilbert, E., Pishniak, D., Torres, J.A., Orr, A., Maclennan, M., Wever, N., Verro, K., 2025. Extreme
536 precipitation associated with atmospheric rivers over West Antarctic ice shelves: insights from
537 kilometre-scale regional climate modelling. The Cryosphere 19, 597–618.

https://doi.org/10.5194/tc-19-597-2025

Gutmann, E.D., Rasmussen, R.M., Liu, C., Ikeda, K., Gochis, D.J., Clark, M.P., Dudhia, J., Thompson, G., 2012. A Comparison of Statistical and Dynamical Downscaling of Winter Precipitation over Complex Terrain. J. Climate 25, 262–281. https://doi.org/10.1175/2011JCLI4109.1

Hong, S.-Y., Noh, Y., Dudhia, J., 2006. A New Vertical Diffusion Package with an Explicit Treatment of Entrainment Processes. Mon. Weather Rev. 134, 2318–2341. https://doi.org/10.1175/MWR3199.1

Horton, R.M., Mankin, J.S., Lesk, C., Coffel, E., Raymond, C., 2016. A Review of Recent Advances in Research on Extreme Heat Events. Curr. Clim. Change Rep. 2, 242–259. https://doi.org/10.1007/s40641-016-0042-x

Huang, N.E., Shen, Z., Long, S.R., Wu, M.C., Shih, H.H., Zheng, Q., Yen, N.-C., Tung, C.C., Liu, H.H., 1998. The empirical mode decomposition and the Hilbert spectrum for nonlinear and non-stationary time series analysis. Proc. R. Soc. Lond. A. 454, 903–995. https://doi.org/10.1098/rspa.1998.0193

Huang, Y., Xue, M., Hu, X., Martin, E., Novoa, H.M., McPherson, R.A., Liu, C., Chen, M., Hong, Y., Perez, A., Morales, I.Y., Ticona Jara, J.L., Flores Luna, A.J., 2024. Increasing frequency and precipitation intensity of convective storms in the Peruvian Central Andes: Projections from convection-permitting regional climate simulations. Quart. J. Royal Meteoro. Soc. 150, 4371–4390. https://doi.org/10.1002/qj.4820

Imran, H.M., Evans, J.P., 2025. Observational uncertainty in the added value of regional climate modelling over Australia. Clim. Dyn. 63, 73. https://doi.org/10.1007/s00382-024-07562-y

IPCC, 2021. Weather and climate extreme events in a changing climate. In climate change 2021: The physical science basis. Contribution of Working Group I to the Sixth Assessment Report of the Intergovernmental Panel on Climate Change. Cambridge University Press, Cambridge, United Kingdom and New York, NY, USA, pp. 1513–1766, https://doi: 10.1017/9781009157896.013.

Jamal, K., Li, X., Chen, Y., Rizwan, M., Khan, M.A., Syed, Z., Mahmood, P., 2023. Bias correction and projection of temperature over the altitudes of the Upper Indus Basin under CMIP6 climate

scenarios from 1985 to 2100. J. Water Clim. Change 14, 2490–2514. https://doi.org/10.2166/wcc.2023.180

Jia, N., Cheng, J., Li, Y., Zheng, L., Song, W., Chen, R., Zhu, A., 2025. China's Yangtze River drought: A cascade of impacts from mountains to sea. Sci. China Earth Sci. 68, 957–962. https://doi.org/10.1007/s11430-024-1521-3

Jiang, Q., Li, W., Fan, Z., He, X., Sun, W., Chen, S., Wen, J., Gao, J., Wang, J., 2021. Evaluation of the ERA5 reanalysis precipitation dataset over Chinese Mainland. J. Hydrol. 595, 125660. https://doi.org/10.1016/j.jhydrol.2020.125660

Kramer, R.J., He, H., Soden, B.J., Oreopoulos, L., Myhre, G., Forster, P.M., Smith, C.J., 2021. Observational evidence of increasing global radiative forcing. Geophys. Res. Lett. 48, e2020GL091585. https://doi.org/10.1029/2020GL091585

Lee, T., Ouarda, T.B.M.J., 2010. Long-term prediction of precipitation and hydrologic extremes with nonstationary oscillation processes. J. Geophys. Res. 115, 2009JD012801. https://doi.org/10.1029/2009JD012801

Lei, X., Gao, L., Ma, M., Wei, J., Xu, L., Wang, L., Lin, H., 2021. Does non-stationarity of extreme precipitation exist in the Poyang Lake Basin of China? J. Hydrol.: Reg. Stud. 37, 100920. https://doi.org/10.1016/j.ejrh.2021.100920

Lin, C., Kjellström, E., Wilcke, R.A.I., Chen, D., 2022. Present and future European heat wave magnitudes: climatologies, trends, and their associated uncertainties in GCM-RCM model chains. Earth Syst. Dynam. 13, 1197–1214. https://doi.org/10.5194/esd-13-1197-2022

Lin, S., Zhang, Y., Sun, S., Guan, X., Jiang, C., Gao, L., 2023. Sensitivity study of WRF parameterization schemes and initial fields on simulation of rainstorm in the Minjiang River basin. Pearl River (in Chinese) 44(10):35-46+61. https://doi: 10.3969/j.issn.1001-9235.2023.10.004

Liu, H., Xiao, P., Zhang, X., Liang, Y., Tang, B., Chen, S., Liu, Y., 2024. Winter snowpack loss increases warm-season compound hot-dry extremes. Commun. Earth Environ. 5, 567. https://doi.org/10.1038/s43247-024-01734-8

Liu, Y., Chen, J., Xiong, L., Xu, C.-Y., 2024. Integrating heterogeneous information for modeling non-stationarity of extreme precipitation in the Yangtze River Basin. J. Hydrol. 645, 132159.

https://doi.org/10.1016/j.jhydrol.2024.132159

Ma, L., Hu, S., Zhou, B., Peng, J., Li, D., 2025. Novel dynamical indices for the variations of the South Asia high in a warming climate. Atmos. Res. 315, 107901. https://doi.org/10.1016/j.atmosres.2024.107901

Mlawer, E.J., Taubman, S.J., Brown, P.D., Iacono, M.J., Clough, S.A., 1997. Radiative transfer for inhomogeneous atmospheres: RRTM, a validated correlated-k model for the longwave. J. Geophys. Res.: Atmos. 102, 16663–16682. https://doi.org/10.1029/97JD00237

Miao, L., Ju, L., Sun, S., Agathokleous, E., Wang, Q., Zhu, Z., Liu, R., Zou, Y., Lu, Y., Liu, Q., 2024. Unveiling the dynamics of sequential extreme precipitation-heatwave compounds in China. npj Clim. Atmos. Sci. 7, 67. https://doi.org/10.1038/s41612-024-00613-5

Min, Y., Huang, W., Ma, M., Zhang, Y., 2021. Simulations in the topography effects of Tianshan Mountains on an extreme precipitation event in the Ili River Valley, China. Atmosphere 12, 750. https://doi.org/10.3390/atmos12060750

Mukherjee, S., Mishra, A.K., Zscheischler, J., Entekhabi, D., 2023. Interaction between dry and hot extremes at a global scale using a cascade modeling framework. Nat. Commun. 14, 277. https://doi.org/10.1038/s41467-022-35748-7

Nerantzaki, S.D., Papalexiou, S.M., Rajulapati, C.R., Clark, M.P., 2023. Nonstationarity in high and low-temperature extremes: Insights from a global observational data set by merging extreme-value methods. Earth's Future 11, e2023EF003506. https://doi.org/10.1029/2023EF003506

Niu, G.-Y., Yang, Z.-L., Mitchell, K.E., Chen, F., Ek, M.B., Barlage, M., Kumar, A., Manning, K., Niyogi, D., Rosero, E., Tewari, M., Xia, Y., 2011. The community Noah land surface model with multiparameterization options (Noah-MP): 1. Model description and evaluation with local-scale measurements. J. Geophys. Res.: Atmos. 116, D12109. https://doi.org/10.1029/2010JD015139

Nordling, K., Fahrenbach, N.L.S., Samset, B.H., 2025. Climate variability can outweigh the influence of climate mean changes for extreme precipitation under global warming. Atmos. Chem. Phys. 25, 1659–1684. https://doi.org/10.5194/acp-25-1659-2025

Patel, R.N., Bonan, D.B., Schneider, T., 2024. Changes in the frequency of observed temperature

extremes largely driven by a distribution shift. Geophys. Res. Lett. 51, e2024GL110707. https://doi.org/10.1029/2024GL110707

Qian, C., 2016. On trend estimation and significance testing for non-Gaussian and serially dependent data: quantifying the urbanization effect on trends in hot extremes in the megacity of Shanghai. Clim. Dyn. 47, 329–344. https://doi.org/10.1007/s00382-015-2838-0

Rahimi, S., Huang, L., Norris, J., Hall, A., Goldenson, N., Risser, M., Feldman, D.R., Lebo, Z.J., Dennis, E., Thackeray, C., 2024. Understanding the cascade: removing GCM biases improves dynamically downscaled climate projections. Geophys. Res. Lett. 51, e2023GL106264. https://doi.org/10.1029/2023GL106264

Ridder, N.N., Ukkola, A.M., Pitman, A.J., Perkins-Kirkpatrick, S.E., 2022. Increased occurrence of high impact compound events under climate change. npj Clim. Atmos. Sci. 5, 3. https://doi.org/10.1038/s41612-021-00224-4

Rigby, R.A., Stasinopoulos, D.M., 2005. Generalized dditive Models for Location, Scale and Shape. J. R. Stat. Soc. C-Appl. 54, 507–554. https://doi.org/10.1111/j.1467-9876.2005.00510.x

Salarijazi, M., Ghorbani, K., Mohammadi, M., Ahmadianfar, I., Mohammadrezapour, O., Naser, M.H., Yaseen, Z.M., 2023. Spatial-temporal estimation of maximum temperature high returns periods for annual time series considering stationary/nonstationary approaches in Iran urban area. Urban Clim. 49, 101504. https://doi.org/10.1016/j.uclim.2023.101504

Samset, B.H., Sand, M., Smith, C.J., Bauer, S.E., Forster, P.M., Fuglestvedt, J.S., Osprey, S., Schleussner, C. - F., 2018. Climate impacts from a removal of anthropogenic aerosol emissions. Geophys. Res. Lett. 45, 1020–1029. https://doi.org/10.1002/2017GL076079

Sauter, C., Fowler, H.J., Westra, S., Ali, H., Peleg, N., White, C.J., 2023. Compound extreme hourly rainfall preconditioned by heatwaves most likely in the mid-latitudes. Weather Clim. Extremes 40, 100563. https://doi.org/10.1016/j.wace.2023.100563

Shang, S., Arnault, J., Zhu, G., Chen, H., Wei, J., Zhang, K., Zhang, Z., Laux, P., Kunstmann, H., 2022. Recent increase of spring precipitation over the three-river headwaters region—water budget analysis based on global reanalysis (ERA5) and ET-tagging extended regional climate modeling. J. Climate 35, 7199–7217. https://doi.org/10.1175/JCLI-D-21-0829.1

Shao, S., Zhang, H., Singh, V.P., Ding, H., Zhang, J., Wu, Y., 2022. Nonstationary analysis of

654 hydrological drought index in a coupled human-water system: Application of the GAMLSS
655 with meteorological and anthropogenic covariates in the Wuding River basin, China. J. Hydrol.
656 608, 127692. https://doi.org/10.1016/j.jhydrol.2022.127692
657 Shu, Z., Jin, J., Zhang, J., Wang, G., Lian, Y., Liu, Y., Bao, Z., Guan, T., He, R., Liu, C., Jing, P.,
658 2024. 1.5℃ and 2.0℃ of global warming intensifies the hydrological extremes in China. J.
659 Hydrol. 635, 131229. https://doi.org/10.1016/j.jhydrol.2024.131229
660 Singh, H., Najafi, M.R., Cannon, A.J., 2021. Characterizing non-stationary compound extreme
661 events in a changing climate based on large-ensemble climate simulations. Clim. Dyn. 56,
662 1389–1405. https://doi.org/10.1007/s00382-020-05538-2
663 Song, X., Zhang, J., Zou, X., Zhang, C., AghaKouchak, A., Kong, F., 2019. Changes in precipitation
664 extremes in the Beijing metropolitan area during 1960–2012. Atmos. Res. 222, 134–153.
665 https://doi.org/10.1016/j.atmosres.2019.02.006
666 Stasinopoulos, D.M., Rigby, R.A., 2007. Generalized Additive Models for Location Scale and
667 Shape (GAMLSS) in R. J. Stat. Soft. 23. https://doi.org/10.18637/jss.v023.i07
668 Sun, F., Roderick, M.L., Farquhar, G.D., 2018. Rainfall statistics, stationarity, and climate change.
669 Proc. Natl. Acad. Sci. U.S.A. 115, 2305–2310. https://doi.org/10.1073/pnas.1705349115
670 Sun, X., Tu, Y., Sun, S., Zhou, X., Jiang, L., Hao, X., Jiang, C., Gao, L., 2025. Identification and
671 spatiotemporal characteristics of compound extreme climate events in the Minjiang River
672 Basin. Water Resour. Hydropower Engineering (In Chinese) 56 (3): 1-14. https://
673 doi:10.13928/j.cnki.wrahe.2025.03.001
674 Talbot, C., Bou-Zeid, E., Smith, J., 2012. Nested mesoscale large-eddy simulations with WRF:
675 performance in real test cases. J. Hydrometeorol. 13, 1421–1441.
676 https://doi.org/10.1175/JHM-D-11-048.1
677 Tapiador, F.J., Navarro, A., Moreno, R., Sánchez, J.L., García-Ortega, E., 2020. Regional climate
678 models: 30 years of dynamical downscaling. Atmos. Res. 235, 104785.
679 https://doi.org/10.1016/j.atmosres.2019.104785
680 Torrez-Rodriguez, L., Goubanova, K., Muñoz, C., Montecinos, A., 2023. Evaluation of temperature
681 and precipitation from CORDEX-CORE South America and Eta-RCM regional climate
682 simulations over the complex terrain of Subtropical Chile. Clim. Dyn. 61, 3195–3221.

https://doi.org/10.1007/s00382-023-06730-w

Van Der Wiel, K., Bintanja, R., 2021. Contribution of climatic changes in mean and variability to monthly temperature and precipitation extremes. Commun. Earth Environ. 2, 1. https://doi.org/10.1038/s43247-020-00077-4

Varga, Á.J., Breuer, H., 2020. Sensitivity of simulated temperature, precipitation, and global radiation to different WRF configurations over the Carpathian Basin for regional climate applications. Clim. Dyn. 55, 2849–2866. https://doi.org/10.1007/s00382-020-05416-x

Varga, Á.J., Breuer, H., 2022. Evaluation of convective parameters derived from pressure level and native ERA5 data and different resolution WRF climate simulations over Central Europe. Clim. Dyn. 58, 1569–1585. https://doi.org/10.1007/s00382-021-05979-3

Wang, S., Chen, X., Yao, H., Ruan, W., Gu, Z., Li, X., Chen, Y., Liu, M., Deng, H., 2024. Separation and spatial variations of typhoon and non-typhoon rainfall at different timescales in typical region of southeast China. Intl. J Climatol. 44, 4611–4628. https://doi.org/10.1002/joc.8599

Wang, Y., Yang, K., Zhou, X., Chen, D., Lu, H., Ouyang, L., Chen, Y., Lazhu, Wang, B., 2020. Synergy of orographic drag parameterization and high resolution greatly reduces biases of WRF-simulated precipitation in central Himalaya. Clim. Dyn. 54, 1729–1740. https://doi.org/10.1007/s00382-019-05080-w

Wu, H., Su, X., Singh, V.P., 2023. Increasing risks of future compound climate extremes with warming over global land masses. Earth's Future 11, e2022EF003466. https://doi.org/10.1029/2022EF003466

Wu, J., Wang, Z., Dong, J., Cui, X., Tao, S., Chen, X., 2023. Robust Runoff Prediction With Explainable Artificial Intelligence and Meteorological Variables From Deep Learning Ensemble Model. Water Resour. Res. 59, e2023WR035676. https://doi.org/10.1029/2023WR035676

Wu, L., Zheng, H., 2023. Regional Climate Effects of Irrigation under Central Asia Warming by 2.0 °C. Remote Sens. 15, 3672. https://doi.org/10.3390/rs15143672

Wu, X., Hao, Z., Zhang, X., Li, C., Hao, F., 2020. Evaluation of severity changes of compound dry and hot events in China based on a multivariate multi-index approach. J. Hydrol. 583, 124580. https://doi.org/10.1016/j.jhydrol.2020.124580

712 Wu, Y., Miao, C., Sun, Y., AghaKouchak, A., Shen, C., Fan, X., 2021. Global observations and
713 CMIP6 simulations of compound extremes of monthly temperature and precipitation.
714 GeoHealth 5, e2021GH000390. https://doi.org/10.1029/2021GH000390
715 Xie, Y., Sun, W., Ren, M., Chen, S., Huang, Z., Pan, X., 2023. Stacking ensemble learning models
716 for daily runoff prediction using 1D and 2D CNNs. Expert Syst. Appl. 217, 119469.
717 https://doi.org/10.1016/j.eswa.2022.119469
718 Xu, W., Liu, Z., Gao, L., Lei, X., Zhang, Y., 2025. Changes in Global Marine Heatwaves in a Non-
719 stationary Climate. Geophys. Res. Lett. 52, e2024GL114497.
720 https://doi.org/10.1029/2024GL114497
721 Xu, Z., Han, Y., Tam, C.-Y., Yang, Z.-L., Fu, C., 2021. Bias-corrected CMIP6 global dataset for
722 dynamical downscaling of the historical and future climate (1979–2100). Sci. Data 8, 293.
723 https://doi.org/10.1038/s41597-021-01079-3
724 Yan, Y., Gao, L., Chen, R., Zhang, C., Ren, L., Zhang, X., Chen, C., 2024. Analysis of Disaster and
725 Damage Process Caused by No. 2305 “Doksuri” Typhoon Disaster Chain in Fuzhou City. J.
726 Catastrophology (In Chinese) 39 (4): 228-234. https://doi: 10. 3969/j. issn. 1000-811X. 2024.
727 04. 033
728 Yang, T., Chen, X., Hamdi, R., Li, L., Cui, F., De Maeyer, P., Duan, W., 2025. Rainfall-driven
729 extreme snowmelt will increase in the Tianshan and Pamir Regions under future climate
730 projection. J. Geophys. Res.: Atmos. 130, e2024JD042323.
731 https://doi.org/10.1029/2024JD042323
732 Yang, T., Chen, X., Hamdi, R., Li, Q., Cui, F., Li, L., Liu, Y., De Maeyer, P., Duan, W., 2024.
733 Assessment of snow simulation using Noah-MP land surface model forced by various
734 precipitation sources in the Central Tianshan Mountains, Central Asia. Atmos. Res. 300,
735 107251. https://doi.org/10.1016/j.atmosres.2024.107251
736 Yang, X., Yan, Y., Zhou, X., Zhu, L., Ma, M., Zhang, J., Chen, Y., Gao, L., 2025. Risk of Compound
737 Typhoon Disaster Chains: Insights from Southeastern China. Int. J. Disaster Risk Sci. 16, 870–
738 887. https://doi.org/10.1007/s13753-025-00674-x
739 Yin, C., Ting, M., Kornhuber, K., Horton, R.M., Yang, Y., Jiang, Y., 2025. CETD, a global
740 compound events detection and visualisation toolbox and dataset. Sci. Data 12, 356.

https://doi.org/10.1038/s41597-025-04530-x

Yin, H., Zhang, X., Wang, F., Zhang, Y., Xia, R., Jin, J., 2021. Rainfall-runoff modeling using LSTM-based multi-state-vector sequence-to-sequence model. J. Hydrol. 598, 126378. https://doi.org/10.1016/j.jhydrol.2021.126378

You, J., Yin, F., Gao, L., 2025. Escalating wind power shortages during heatwaves. Commun. Earth Environ. 6, 245. https://doi.org/10.1038/s43247-025-02239-8

Zeng, J., Li, H., Sun, B., Chen, H., Wang, H., Zhou, B., Duan, M., 2024. Summertime compound heat wave and drought events in China: interregional and subseasonal characteristics, and the associated driving factors. Environ. Res. Lett. 19, 074046. https://doi.org/10.1088/1748-9326/ad5576

Zeng, J., Zhang, S., Zhou, S., Obulkasim, O., Zhang, H., Lu, X., Dai, Y., 2024. Comparison of the risks and drivers of compound hot-dry and hot-wet extremes in a warming world. Environ. Res. Lett. 19, 114026. https://doi.org/10.1088/1748-9326/ad7617

Zhang, C., Wang, Y., Hamilton, K., 2011. Improved Representation of Boundary Layer Clouds over the Southeast Pacific in ARW-WRF Using a Modified Tiedtke Cumulus Parameterization Scheme*. Mon. Weather Rev. 139, 3489–3513. https://doi.org/10.1175/MWR-D-10-05091.1

Zhang, J., Zhao, T., Zhang, Juanjuan, Ren, Y., Li, Z., 2024. Changes in compound temperature and precipitation extremes from combined effects of multiple circulation factors over China. J. Hydrol. 642, 131884. https://doi.org/10.1016/j.jhydrol.2024.131884

Zhang, M., Han, Y., Xu, Z., Guo, W., 2024. Assessing Climate Extremes in Dynamical Downscaling Simulations Driven by a Novel Bias-Corrected CMIP6 Data. J. Geophys. Res.: Atmos. 129, e2024JD041253. https://doi.org/10.1029/2024JD041253

Zhang, W., Furtado, K., Wu, P., Zhou, T., Chadwick, R., Marzin, C., Rostron, J., Sexton, D., 2021. Increasing precipitation variability on daily-to-multiyear time scales in a warmer world. Sci. Adv. 7, eabf8021. https://doi.org/10.1126/sciadv.abf802

Zhang, Y., Deng, C., Xu, W., Zhuang, Y., Jiang, L., Jiang, C., Guan, X., Wei, J., Ma, M., Chen, Y., Peng, J., Gao, L., 2025. Long-term variability of extreme precipitation with WRF model at a complex terrain River Basin. Sci. Rep. 15, 156. https://doi.org/10.1038/s41598-024-84076-x

Zhao, T., Xiong, S., Tian, Y., Wu, Y., Li, B., Chen, X., 2024. Compound dry and hot events over

major river basins of the world from 1921 to 2020. Weather Clim. Extremes 44, 100679. https://doi.org/10.1016/j.wace.2024.100679

Zhou, P., Tang, J., Ma, M., Ji, D., Shi, J., 2024. High resolution Tibetan Plateau regional reanalysis 1961-present. Sci. Data 11, 444. https://doi.org/10.1038/s41597-024-03282-4

Zheng, M., Chen, X., Ruan, W., Yao, H., Gu, Z., Geng, K., Li, X., Deng, H., Chen, Y., Liu, M., 2023. Spatiotemporal variation of water cycle components in Minjiang River Basin based on a correction method for evapotranspiration products. J. Hydrol.: Reg. Stud. 50, 101575. https://doi.org/10.1016/j.ejrh.2023.101575

Zscheischler, J., Westra, S., Van Den Hurk, B.J.J.M., Seneviratne, S.I., Ward, P.J., Pitman, A., AghaKouchak, A., Bresch, D.N., Leonard, M., Wahl, T., Zhang, X., 2018. Future climate risk from compound events. Nature Clim. Change 8, 469–477. https://doi.org/10.1038/s41558-018-0156-3